2023 IEEE/RSJ International Conference on Intelligent Robots and Systems (IROS)
October 1-5, 2023. Detroit, USA

Canfly: A Can-sized Autonomous Mini Coaxial Helicopter

Neng Pan, Rui Jin, Chao Xu, and Fei Gao

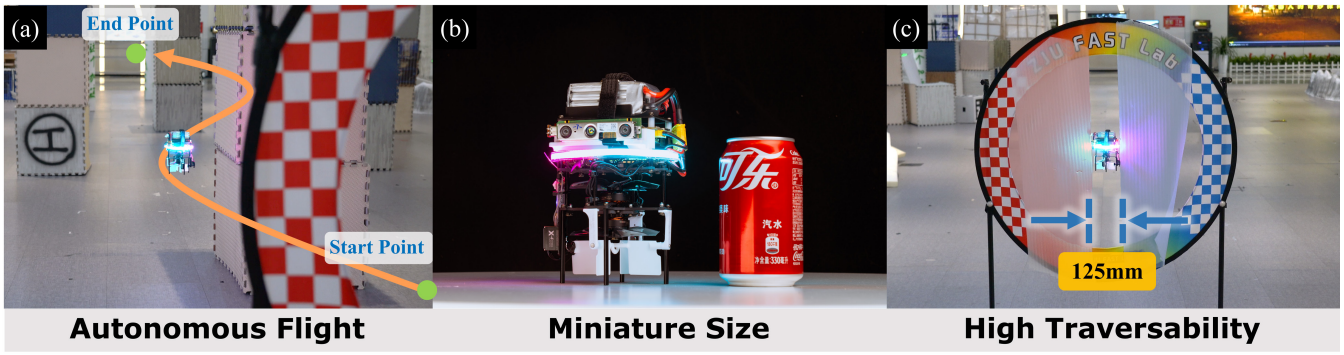

Fig. 1: The proposed coaxial helicopter (a) autonomously navigates through an unknown cluttered environment, (b) possesses a miniature size slightly larger than a can of soda, (c) deftly crosses through a narrow gap of $125mm$ wide.

***Abstract*— The development of autonomous rotary-wing UAVs has shown an evident tendency in miniaturization. However, the side effects brought by miniaturization, such as decreased load capability, shorter flight duration and reduced autonomous ability, seriously hinder its process. In this paper, we first investigate the configurations of different rotary-wing aircraft and optimize the configuration selection. Afterward, with several elaborate mechanisms contributing to the miniaturization, we present the hardware design and control strategy of a mini coaxial helicopter, which is 62% smaller than the state-of-the-art autonomous mini quadrotor so far in collision area [1]. Meanwhile, abundant experiments reveal that it achieves impressive traversability and is capable of conducting autonomous tasks in unknown dense scenarios, while maintaining satisfactory performance regarding loadability and flight duration.**

I. Introduction

In recent years, due to rotary-wing UAVs' hovering capability and impressive agility, they have attracted significant attention across numerous fields, such as aerial photography, rescue operation, collaborative exploration, and formation shows. Meanwhile, the development of UAVs has shown an evident tendency in miniaturization [1]–[4], because the smaller size brings higher mobility, greater traversability, and enhanced safety, thus broadening their application. For example, the ruins after an earthquake are too rugged and dense with obstacles for any ground vehicles or medium-sized UAVs to pass through, while agile mini UAVs can squeeze into the debris and deliver hope for the victims. However, miniaturization also brings challenges, including weaker load capability, shorter flight duration and poorer autonomous ability.

To explore the boundary of miniaturization without sacrificing the flight duration and autonomous ability, an elaborate investigation and thorough design of the hardware configuration are essential. Thanks to quadrotors' compact mechanism and simple control strategy, previous researchers have developed several impressive mini quadrotor systems [1, 3, 4]. However, quadrotors are not the best choice for miniaturization. In the later discussion in Sec. III-A, we demonstrate that helicopters enjoy the highest power efficiency among all kinds of rotary-wing aircraft.

So it's an intuitive idea to draw inspiration from the development of helicopters. During the last few decades, we have seen various configurations of helicopters [2], all showing great potential in different fields. However, most of them suffer from complicated mechanisms, poor controllability or high energy consumption, bringing great difficulties to miniaturization, as discussed in Sec. II.

Based on the reflection of previous works, we develop a mini configuration of UAVs. We name it as Canfly, meaning it has a similar size to a soda can, as shown in Fig. 1(b). Sufficient work is made to minimize Canfly's size, while guaranteeing its loadability and flight duration. The dynamic model and control strategy are presented later in Sec. V. Finally, in Sec.VI Canfly is challenged to navigate through an unknown environment setup with dense obstacles and cross through a narrow gap of $125mm$ wide, revealing its satisfactory controllability and impressive traversability.

We summarize our contributions as follows:

1) A comprehensive investigation into different kinds of rotary-wing UAV configuration, supporting the view that coaxial helicopters based on control surfaces are the most suitable configuration for mini autonomous UAVs.
2) The hardware design and control strategy of a coaxial

All authors are with the State Key Laboratory of Industrial Control Technology, Zhejiang University, Hangzhou 310027, China and Huzhou Institute, Zhejiang University, Huzhou 313000, China. This work was supported by the National Natural Science Foundation of China under grant no. 62003299 and the Fundamental Research Funds for the Central Universities.
E-mail:{panneng_zju, fgaoaa}@zju.edu.cn

2023 IEEE/RSJ International Conference on Intelligent Robots and Systems (IROS) | 978-1-6654-9190-7/23/$31.00 ©2023 IEEE | DOI: 10.1109/IROS55552.2023.10341490

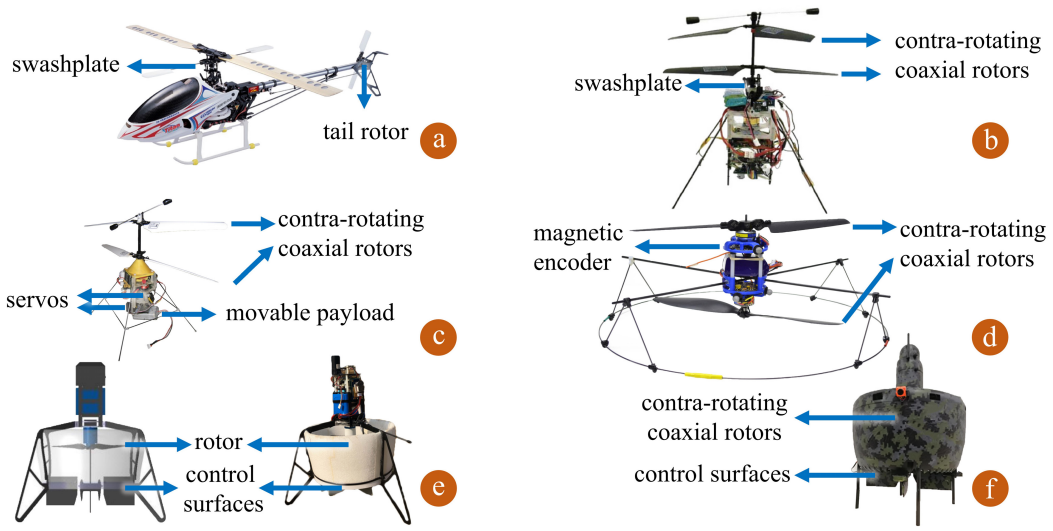

Fig. 2: (a) A conventional electric helicopter with a swashplate and a tail rotor. (b) A coaxial helicopter without a tail rotor proposed by Schafroth et al. [5]. (c) A coaxial helicopter controlled by moving the center of gravity, proposed by Bouabdallah et al. [6, 7]. (d) A coaxial helicopter with only two motors proposed by Paulos et al. [8, 9]. (e) A homotaxial helicopter controlled by control surfaces, proposed by Deng et al. [10]. (f) A coaxial helicopter controlled by control surfaces, proposed by Deng et al. [11].

helicopter based on control surfaces, which is 62% smaller than the state-of-the-art smallest autonomous UAV platform in collision area [1].

3) Sufficient experiments validating the controllability, autonomous ability and traversability of Canfly.

II. Related Works

A. Miniaturization Process of Quadrotors

Many researchers have explored the miniaturization of autonomous UAVs [1, 3, 4]. One of the representative works is the Crazyflie series proposed by Giernacki et al. [4]. Crazyflie is a nano quadrotor whose minimum circumscribed circle's diameter is $137mm$, which is very impressive for an autonomous UAV. However, due to the usage of coreless DC motors, the maximum payload of Crazyflie is limited to $15g$. The poor load capability tightly restricts the introduction of vision sensors with higher precision, onboard computers with higher computational power, or batteries with larger capacity, which is necessary for most autonomous tasks. As a result, Crazyflies can only conduct low-level autonomous tasks, waypoints tracking for example.

To make the UAVs qualified for high-level autonomous tasks, researchers [3] equip a brushless-motor-driven quadrotor with a DJI Manifold2-C onboard computer and a Realsense D435 stereo camera. This quadrotor is $377mm$ wide in circumscribed circle's diameter, and capable of carrying a payload up to $1kg$. Later, Zhou et al. [1] integrate the system into a more compact configuration whose width is $188mm$ and the payload is $200g$, making it the smallest autonomous UAV system qualified for high-level tasks so far.

However, previous works tend to dig into the configurations of quadrotors. In the later discussion in Sec. III-A, we prove that helicopters are the preferred configurations for mini UAVs, and we should focus more on the development of helicopters.

B. Development of Helicopters

During the last few decades, various configurations of helicopters [2] have sprung up, all showing great potential in different fields. The most commonly seen helicopter [12], as shown in Fig. 2(a), consists of a swashplate and a tail rotor. The swashplate is a delicate mechanism that can control the orientation of the thrust vector, but its complicated structure makes it rather challenging to be applied in mini UAVs. Moreover, the extra tail rotor also increases the body length, bringing more difficulty to miniaturization.

To get rid of the tail rotor, researchers have come up with a coaxial helicopter with a swashplate [5, 13], as shown in Fig. 2(b). Its contra-rotating coaxial rotors can provide thrust while generating little reaction torque and gyroscopic torque, which means it can achieve full controllability of yaw without the help of the tail rotor. However, the generation of pitch torque and roll torque still relies on the cyclic control of the swashplate, making the miniaturization process still challenging. On the other hand, the integrated contra-rotating rotors present an additional complexity to the mechanism.

To avoid the introduction of the swashplate, Bouabdallah et al. [6, 7] propose a coaxial helicopter whose steering is achieved by controlling the center of gravity with two servos, as shown in Fig. 2(c). Such designs greatly reduce the size of the vehicle, but the price is that it suffers from little control margin and poor controllability.

Other researchers propose a coaxial helicopter that can emulate full actuation over forces and torques using only two motors [8, 9], as shown in Fig. 2(d). It is realized by exciting the motors with a cyclic flapping response to control the orientation of the thrust vector. Unfortunately, the motors will overheat during high-frequency accelerations and decelerations, where much energy is wasted. Moreover, the introduction of magnetic encoders in this configuration is not a practical choice for miniaturization, either.

Another way to gain pitch and roll torque is by adopting aerodynamic control surfaces. Researchers [10, 14] discuss the design and control strategy of a homotaxial helicopter that consists of one motor and four individual control surfaces, as shown in Fig. 2(e). The motor provides the thrust and the control surfaces provide the torque in roll, pitch and yaw. Researchers [11] propose a similar helicopter with coaxial rotors, which can naturally get rid of the reaction torque and gyroscopic torque, as shown in Fig. 2(f). Such designs based on control surfaces abandon all complicated transmission mechanisms, have few fatal drawbacks, and are in our favor for miniaturization. We will discuss the difference between them in detail in Sec. III-B.

III. Configuration Comparison and Optimazation

A. Efficiency of Different Configurations of Rotary-Wings

As mentioned above, the main purpose of the hardware design is to minimize the valid size while maintaining satisfactory hover efficiency. In this paper, we take the minimum circumscribed circle's area of the horizontal projection as the valid size of a UAV, because the vehicle is modeled as a sphere or a circle in most path planning algorithms [15, 16]. On the other hand, we focus more on the horizontal area because there is more vertical free space than horizontal free space in most structured and unstructured scenarios, cities with dense buildings, narrow windows and forests for example. In this section, we will demonstrate that the helicopters enjoy the maximum hover efficiency among the commonly used configurations of rotary-wing aircraft.

According to the momentum theory [17] and the verification in work [18], we know that the ideal power P of a rotor to produce a thrust F_T is

$$P(F_T) = F_T\sqrt{\frac{F_T}{2S\rho}}, \tag{1}$$

where S is the swept area of the rotor, and ρ is the density of air. For a rotary-wing aircraft with n rotors and total mass of m_l, the hover efficiency E_h is

$$E_h(n) = \frac{MASS}{POWER} = \frac{m_l}{n \cdot P(m_l g/n)} = \sqrt{\frac{2S n\rho}{m_l g^3}}. \tag{2}$$

Given a circumscribed circle of radius R, the radius r of the helicopter's propeller is simply R. As for a multicopter whose number of rotors $n \geq 2$, assume the rotors are tangent to the adjacent rotors[1], which should maximize the valid rotor area. The circumstance is shown in Fig. 3, where O is the center of the circumscribed circle, and $O_k(k \in N_+)$ is the center of the k^{th} rotor.

As for $O_1O_2O_3...O_n$ is an equilateral polygon, we know

$$\begin{aligned} \angle O_2OO_3 &= \frac{2\pi}{n}, \\ OO_2 &= \frac{O_2O_3}{2\sin(\pi/n)} = \frac{r}{\sin(\pi/n)}. \end{aligned} \tag{3}$$

[1]In practice, we have to leave some spaces between each rotor, which will result in a less valid rotor area for multicopters.

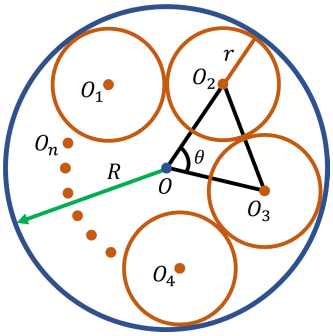

Fig. 3: Circumscribed circle of a multicopter with n rotors. O is the center of the circumscribed circle, and $O_k(k \in N_+)$ is the center of the k^{th} rotor.

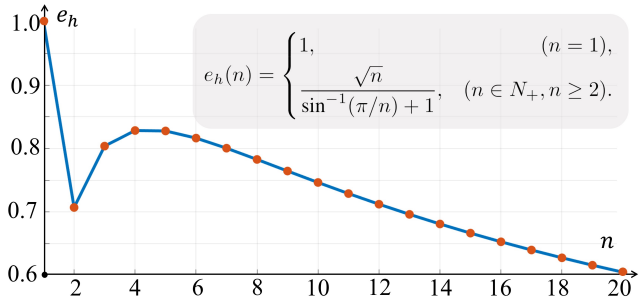

Fig. 4: The figure of $e_h(n)$, a dimensionless coefficient indicating the hover efficiency of a rotary-wing aircraft with n rotors.

Together with $R = OO_2 + r, (n \in N_+, n \geq 2)$, we have

$$r = \begin{cases} R, & (n=1), \\ \dfrac{R}{1+\sin^{-1}(\pi/n)}, & (n \in N_+, n \geq 2). \end{cases} \tag{4}$$

Given $S = \pi r^2$, substituting Equ. (4) to Equ. (1) gives us

$$E_h(n) = \begin{cases} \sqrt{\dfrac{2\pi\rho}{m_l g^3}}R, & (n=1), \\ \sqrt{\dfrac{2\pi\rho}{m_l g^3}}R \cdot \dfrac{\sqrt{n}}{\sin^{-1}(\pi/n)+1}, & (n \in N_+, n \geq 2). \end{cases} \tag{5}$$

Assuming the load m_l is the same for every multicopter, the term $\sqrt{2\pi\rho/m_l g^3}R$ is a constant value, and Equ. (5) indicates that the hover efficiency is proportional to

$$e_h(n) = \begin{cases} 1, & (n=1), \\ \dfrac{\sqrt{n}}{\sin^{-1}(\pi/n)+1}, & (n \in N_+, n \geq 2). \end{cases} \tag{6}$$

By drawing the figure of $e_h(n)$ shown in Fig. 4, we know $e_h(n)$ is a function whose two maximum values locate in

$$\begin{aligned} e_{hmax1} &= e_h(1) = 1, \\ e_{hmax2} &= e_h(4) = \frac{2}{\sqrt{2}+1} \approx 0.828, \end{aligned} \tag{7}$$

which indicates that the hover efficiency of a helicopter is higher than any other rotary-wing aircraft.

Coaxial Helicopter
2 Motors and **2 Servos**

Homotaxial Helicopter
1 Motor and **4 Servos**

Fig. 5: The comparison between a coaxial helicopter and a homotaxial helicopter.

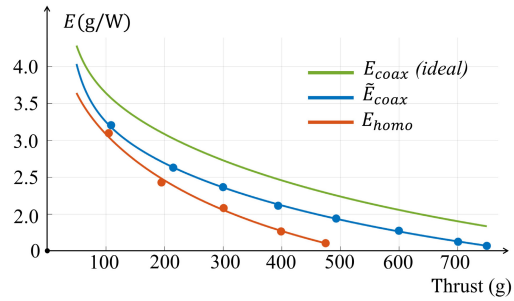

Fig. 6: The hover efficiency of ideal coaxial rotor, corrected coaxial rotors and a homotaxial rotor at different thrusts.

B. Coaxial Helicopters vs. Homotaxial Helicopters

As we discuss in Sec. II and Sec. III-A, we find out that helicopters based on control surfaces are the preferred choice for mini UAVs. In this subsection, we discuss whether a homotaxial one or a coaxial one is a more suitable configuration for the desired mini autonomous UAV.

The typical coaxial helicopter design consists of two motors and two servos, and the typical homotaxial helicopter design consists of one motor and four servos, as shown in Fig. 5. In a coaxial helicopter, the contra-rotating rotors provide thrust and yaw torque, and the control surfaces provide roll and pitch torque. The opposite control surfaces move in the same direction, so they can be driven by the same servo. While in a homotaxial helicopter, the reaction torque of the rotor has to be balanced by the control surfaces, so the opposite control surfaces may move in different directions, which means they have to be driven individually. Thus we know that coaxial helicopters have fewer actuators and a more compact mechanism than homotaxial helicopters.

Meanwhile, coaxial helicopters enjoy higher hover efficiency and maximum thrust than homotaxial helicopters. Assume that a coaxial helicopter and a homotaxial helicopter have the same mass m and propeller radius R. Rewrite Equ. (5) as

$$E_h(m_l) = \sqrt{\frac{2\pi\rho}{g^3}} R \cdot \frac{1}{\sqrt{m_l}}. \tag{8}$$

According to Equ. (8), we know $E_h(m_l)$ is a decreasing function with respect to the load m_l. The power of the coaxial helicopter P_{coax} is the sum of the two rotors whose load is $m/2$,

$$P_{coax}(m) = 2 \cdot \frac{\frac{m}{2}}{E_h(\frac{m}{2})} = \frac{m}{E_h(\frac{m}{2})}. \tag{9}$$

$$E_{coax}(m_l) = E_h(\frac{m_l}{2}). \tag{10}$$

As for the homotaxial helicopter, the power is simply

$$P_{homo}(m) = \frac{m}{E_h(m)}, \; E_{homo}(m_l) = E_h(m_l). \tag{11}$$

Combining Equ. (10) and Equ. (11) gives

$$E_{coax}(m_l) = \sqrt{2} E_{homo}(m_l), \tag{12}$$

which indicates coaxial helicopters are 41.4% more efficient than homotaxial helicopters ideally.

C. Aerodynamic Power Loss and Rotor Efficiency

In practice, we know there exists a nonnegligible aerodynamic disturbance between the coaxial rotors, which will result in reduced power efficiency [19]. If we take the aerodynamic power loss η_{AL} into consideration, we have the corrected hover efficiency $\widetilde{E}_{coax}$ and power of the coaxial helicopter $\widetilde{P}_{coax}$,

$$\widetilde{P}_{coax}(m) = \frac{m}{E_h(\frac{m}{2})\,(1-\eta_{AL})}, \tag{13}$$

$$\widetilde{E}_{coax}(m) = E_h(\frac{m}{2})\,(1-\eta_{AL})\,. \tag{14}$$

To measure η_{AL}, we conduct an experiment and measure the power of the homotaxial rotor and coaxial rotors at different thrusts. The motor and propeller setup is presented in Sec. IV. Afterward, we use a second-order polynomial to fit the hover efficiency with respect to the thrust and calculate the ideal coaxial hover efficiency according to Equ. (10). The result is shown in Fig. 6.

From the result, we know that η_{AL} is around 13.8% in our configuration, and the corrected coaxial hover efficiency $\widetilde{E}_{coax}$ is 19.5% higher than the homotaxial helicopter's efficiency E_{homo}. Furthermore, the experiment also reveals that the maximum thrust of the coaxial rotors is 58.2% higher than the single rotor, providing abundant thrust for aggressive flight and extra payloads.

IV. Hardware Design and Implementation

Based on the reflection of previous works in Sec. II and analysis in Sec. III, we know that coaxial helicopters based on control surfaces are the most suitable configuration for the desired mini autonomous UAVs. In this section, we present our implementation and design details of the mini coaxial helicopters Canfly.

A. Hardware Implementation

The illustration of the hardware is shown in Fig. 7. The motors are mounted on the same carbon fiber board, where a 3D print component with counter bores is used to avoid the interference of bolts. Compared with conventional integrated contra-rotating motors [5]–[7, 11, 13] where the two motors share the same shaft, such split-type installation can greatly simplify the structure and can be applied to any kind of commercial motors. To avoid interference between

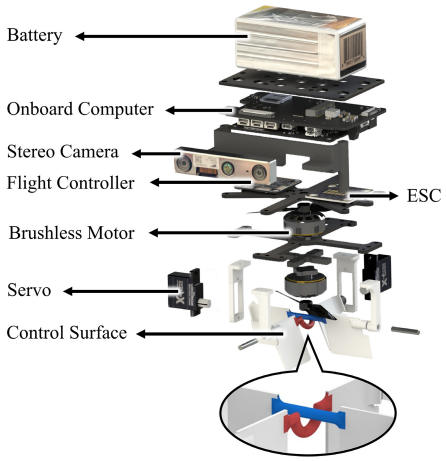

Fig. 7: Illustration of the proposed system's hardware.

TABLE I: Weight and model of each component

Component	Model	Weight (g)
Battery	GNB 1700mAh Li-Hv 4S	160
Onboard computer	NVIDIA Xavier NX	72
Motor	T-Motor F2004	65
Stereo camera	Intel Realsense D430	30
Control surface	3D print	20
Servo	BlueArrow X-4	15
Frame	Carbon fiber	15
Bolts&wires		10
Flight controller	Holybro Kakute Mini	8
ESC	Holybro Tekko32 45A	7
Propeller	Gemfan D76	6
Total		***408***

the two control surfaces while not increasing the height of the vehicle, we bend one of the control surfaces' connecting shafts, as the red and blue highlights in Fig. 7 show.

The total weight of Canfly is $408g$, and the maximum payload is $150g$. The weight and model of each component are listed in Table. I. The flight duration is up to 8 minutes, which is satisfactory for such a mini vehicle with a relatively large payload.

B. Ductless Design

Other helicopters with larger sizes tend to adopt a duct to increase the hover efficiency [10, 11, 14]. However, in this work we discard the duct design mainly based on the following reasons. From work [20] we know the gap between the propeller's tip and the duct's inwall has to be smaller than 3% of the propeller's height to provide a beneficial effect on the system, which in our case is

$$4mm * 3\% = 0.12mm.$$

However, the typical precision of 3D printing is around $0.2mm$, which makes manufacturing rather hard. On the other hand, a slight deformation can easily destroy the delicate gap and leads to a crush, weakening the robustness of the system. Finally, the proposed system is mainly designed for hovering and low-speed cruising, where the duct introduces much air drag while providing little lift force. In conclusion, the duct design is not practical or beneficial to the proposed system with miniature size.

C. Size and Efficiency Comparison

In this subsection, we compare the valid size described in Sec. III-A as well as hover efficiency between Canfly and the state-of-the-art mini UAV system that shares the similar autonomous ability to Canfly [1].

The diameter of the minimum circumscribed circle of Canfly is $116mm$, while Zhou's is $188mm$. The area of the valid collision size of Canfly is 62% less than Zhou's. The illustration is shown in Fig. 8.

As for the hover efficiency, we can calculate it with the battery capacity C, voltage U, flight duration T and total weight m, which can be found in the corresponding paper,

$$E = \frac{UC}{Tm}. \tag{15}$$

The hover efficiency of Zhou's is $2.50g/W$, while Canfly's is $2.16g/W$, indicating that our system can achieve similar hover efficiency with remarkably reduced size.

V. Control

A. Dynamic Model

We introduce two frames for later discussion: body frame ($\mathbf{x_b} - \mathbf{y_b} - \mathbf{z_b}$) and FLU (Forward- Left- Up) world frame ($\mathbf{x_w} - \mathbf{y_w} - \mathbf{z_w}$).

Assume that the aerodynamic forces generated by the control surfaces are horizontal and the vertical drag part is relatively small and can be neglected.

The force analysis is shown in Fig.9, where CoM is the center of mass, f is the collective thrust, F_{CS_i} is the horizontal force generated by the control surfaces, α, β are the angle of the control surfaces respective to $\mathbf{z_b}$, and H is the vertical distance between CoM and control surfaces.

Consider the state of the vehicle $\mathbf{x} = \{\mathbf{r}, \mathbf{R}\}$, where $\mathbf{r}$ is the position of the vehicle's center of mass in the world frame, and $\mathbf{R}$ is the rotation of the body with respect to the world frame. The input is $\mathbf{u} = \{f, \boldsymbol{\tau}\}$, where f is the collective thrust, and $\boldsymbol{\tau}$ is the torque generated by the actuators. Then we have the dynamic model based on Newton-Euler Equation,

$$m\ddot{\mathbf{r}} = -mg\mathbf{e_3} + f\mathbf{R}\mathbf{e_3} + \mathbf{R}\mathbf{F}_{CS}, \tag{16}$$

$$\mathbf{J}\dot{\boldsymbol{\omega}} = \boldsymbol{\tau} - \boldsymbol{\omega} \times \mathbf{J}\boldsymbol{\omega}. \tag{17}$$

In Equ. (16), m is the total mass of the vehicle, g is the gravitational acceleration, $\mathbf{e_3} = (0, 0, 1)^T$, and $\mathbf{F}_{CS}$ is the force generated by the control surfaces in the body frame. In Equ. (17), $\mathbf{J}$ is the inertia matrix, $\boldsymbol{\omega}$ is the angular rate in body frame.

B. Control Surface

In the proposed system, we adopt two flat planes driven by the servos as control surfaces to generate torque in $\mathbf{x_b}$ and

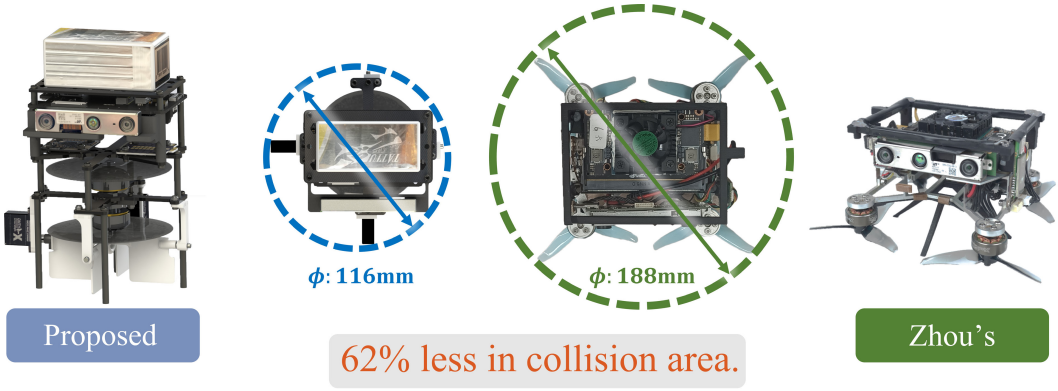

Fig. 8: Comparison with Zhou's quadrotor platform [1], the smallest UAV system so far that share similar autonomous ability with our system. The area of the valid collision size of the proposed system is 62% less than Zhou's.

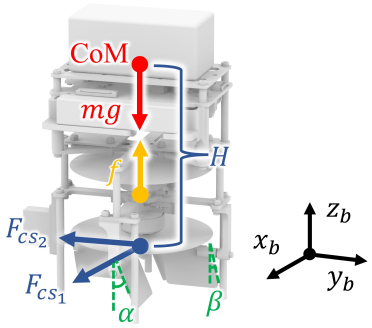

Fig. 9: The force analysis and frame definition of the proposed system.

$\mathbf{y_b}$. According to the work [21], we know the force acting on the control surface can be expressed as

$$F_{CS} = \frac{1}{2}\rho {V_a}^2 S C_L, \tag{18}$$

where ρ is the density of the air, V_a is the velocity of the inflow air, S is the platform area of the control surface, and C_L is the aerodynamic coefficient.

Assuming that the vehicle travel at a low speed and the velocity of the wind can be ignored, we know that V_a equals the speed of the airflow accelerated by the propellers. On the other hand, according to [21] we know the thrust generated by the propeller is proportional to the square of the accelerated airflow's speed ,

$$f = K_v {V_a}^2, \tag{19}$$

where K_v is a constant coefficient.

Assume that the angle of control surfaces θ is small, which is acceptable for low-speed traveling, the aerodynamic coefficients C_L can be linearized by Taylor expansion as,

$$C_L(\theta) = C_{L0} + C_{L\theta}\theta, \tag{20}$$

where C_{L0} is the value of C_L when $\alpha = 0$, and $C_{L\theta}$ is a constant coefficient. Note that $C_{L0} = 0$, because the control surface generates no force when it is vertical, we can rewrite Equ. (20) as

$$C_L(\theta) = C_{L\theta}\theta. \tag{21}$$

Combine Equ. (18), Equ. (19) and Equ. (21), we can conclude that F_{CS} is proportional to the product of θ and f,

$$F_{CS} = K_{CS} f\theta, \;\; K_{CS} = \frac{\rho S C_{L\theta}}{2K_v}. \tag{22}$$

where K_{CS} is a constant coefficient that can be identified in static conditions. This way, the $\mathbf{F}_{CS}$ in Equ. (16) can be defined as

$$\mathbf{F}_{CS} = \left[K_{CS} f\beta, \;\; K_{CS} f\alpha, \;\; 0\right]^T \tag{23}$$

C. Mixer

We use $\mathbf{u} = [f, \boldsymbol{\tau}]^T$ to denote the control input. Given the standard motor model,

$$f_i = K_F {\omega_i}^2, \quad \tau_i = K_M {\omega_i}^2, \tag{24}$$

where f_i is the produced force, τ_i is the reaction torque, ω_i is the motor's angular velocity, K_F is the thrust coefficient and K_M is the reaction torque coefficient, we have

$$\mathbf{u} = \begin{bmatrix} K_F & K_F & 0 & 0 \\ 0 & 0 & K_{CS}H & 0 \\ 0 & 0 & 0 & K_{CS}H \\ K_M & -K_M & 0 & 0 \end{bmatrix} \begin{bmatrix} {\omega_u}^2 \\ {\omega_l}^2 \\ \alpha u_0 \\ \beta u_0 \end{bmatrix}, \tag{25}$$

where ω_u is the angular velocity of the upper motor, and ω_l is the angular velocity of the lower motor.

From Equ. (25), we can derive the actuator output

$$\begin{aligned} \omega_u &= \sqrt{\frac{1}{2}\left(\frac{u_0}{K_F} + \frac{u_3}{K_M}\right)}, \\ \omega_l &= \sqrt{\frac{1}{2}\left(\frac{u_0}{K_F} - \frac{u_3}{K_M}\right)}, \\ \alpha &= \frac{u_1}{K_{CS} H u_0}, \\ \beta &= \frac{u_2}{K_{CS} H u_0}. \end{aligned} \tag{26}$$

D. Attitude Control

We use a cascade control structure to control the attitude, as shown in Fig. 10. The attitude-angular-rate loop is a proportional controller based on the quaternion error described in [22], and the angular-rate-torque loop is a PID controller.

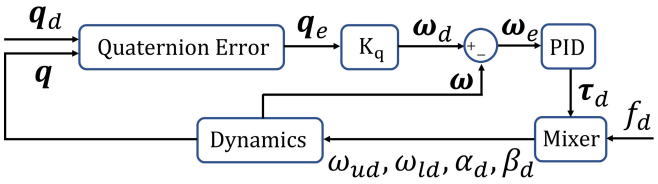

Fig. 10: The control pipeline of the proposed system's attitude control, where a cascade PID controller is applied.

Firstly, we obtain the quaternion $\mathbf{q}$ and angular velocity $\boldsymbol{\omega}$ of the vehicle from the IMU, and calculate the quaternion error $\mathbf{q}_e$ between $\mathbf{q}$ and desired quaternion $\mathbf{q}_d$,

$$\mathbf{q}_e = \mathbf{q}^{-1}\mathbf{q}_d. \tag{27}$$

Next, we calculate the desired angular rate $\boldsymbol{\omega}_d$ using the proportional gain $\mathbf{K}_q$,

$$\mathbf{K}_q = \text{diag}(K_{q1}, K_{q2}, K_{q3}), \tag{28}$$

$$\boldsymbol{\omega}_d = \mathbf{K}_q \text{sgn}(\mathbf{q}_{e,0})\mathbf{q}_{e,1:3}, \tag{29}$$

where

$$\text{sgn}(x) = \begin{cases} 1, & (x \geq 0), \\ -1, & (x < 0). \end{cases} \tag{30}$$

Afterwards, we calculate the desired torque $\boldsymbol{\tau}_d$ using PID gains $\{\mathbf{K}_{P\omega}, \mathbf{K}_{I\omega}, \mathbf{K}_{D\omega}\}$

$$\begin{aligned} \mathbf{K}_{P\omega} &= \text{diag}(K_{P\omega 1}, K_{P\omega 2}, K_{P\omega 3}), \\ \mathbf{K}_{I\omega} &= \text{diag}(K_{I\omega 1}, K_{I\omega 2}, K_{I\omega 3}), \\ \mathbf{K}_{D\omega} &= \text{diag}(K_{D\omega 1}, K_{D\omega 2}, K_{D\omega 3}), \end{aligned} \tag{31}$$

$$\boldsymbol{\tau}_d = \left(\mathbf{K}_{P\omega} + \mathbf{K}_{I\omega}\frac{1}{s} + \mathbf{K}_{D\omega}s\right)(\boldsymbol{\omega}_d - \boldsymbol{\omega}). \tag{32}$$

Together with the desired thrust f_d, we can obtain the desired actuator output $\{\omega_{ud}, \omega_{ld}, \alpha_d, \beta_d\}$ according to the mixer in Equ. (26).

E. Trajectory Tracking

In the research for trajectory tracking of quadrotors, a technique called differential flatness is widely used, which means the states and the inputs of the vehicle can be written as algebraic functions of some carefully selected flat outputs and their derivatives. This can help simplify the control and planning process.

In our case, the combined external forces

$$\mathbf{f}_{ex} = f\mathbf{R}\mathbf{e_3} + \mathbf{R}\mathbf{F}_{CS}, \tag{33}$$

is not always aligned with $\mathbf{z}_b$ of the body. However, the $\mathbf{F}_{CS}$ term is relatively small with respect to the thrust, so it's reasonable and practical to assume $\mathbf{f}_{ex}$ is parallel to $\mathbf{z}_b$. This way, the dynamic of the proposed system is the same as quadrotors' and quadrotors' derived property of differential flatness can be directly applied [23], equipping Canfly with the compatibility for the popular path planners designed for quadrotors [1, 15].

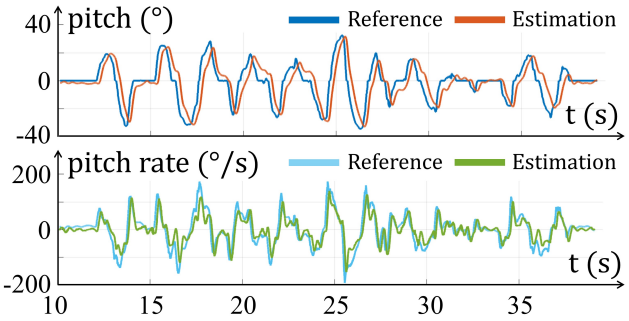

Fig. 11: The result of pitch and pitch rate tracking.

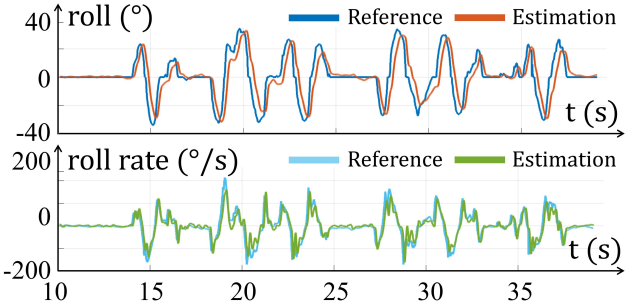

Fig. 12: The result of roll and roll rate tracking.

VI. Experiments

A. Attitude Control Validation

In this experiment, we validate the proposed system's attitude control performance. The attitude setpoint signal is given by a remote controller, and the control series is an imitation of a typical aggressive flight, where the maximum pitch angle and roll angle can reach up to $34°$. The results are shown in Fig. 11, Fig. 12 and Fig. 13.

From the result we can tell the drone can track the attitude series well. However, the delay between the estimation and reference is around $180ms$, which is relatively big compared with typical quadrotors (around $50ms \sim 100ms$). This is mainly brought by the dynamics of the servos where a pure delay is introduced, and stands as a common problem in most servo-based aircrafts.

B. Autonomous Navigation in Unknown Scenarios

In this experiment, we validate the proposed system's autonomous ability. The environment is set up with dense obstacles and the drone is demanded to travel $15m$ ahead at the maximum speed of $1m/s$. The localization is given by the visual-inertial-odometry system VINS-Fusion [24], and the local planner is Ego-Planner [16]. The illustration of the environment and the navigation path is shown in Fig. 1(a). The position tracking error results are shown in Fig.14, and the $RMSE$ is $0.070m$.

C. Crossing a Narrow Gap

In this experiment, we have the drone cross a narrow gap of $125mm$ wide, even shorter than the height of a typical

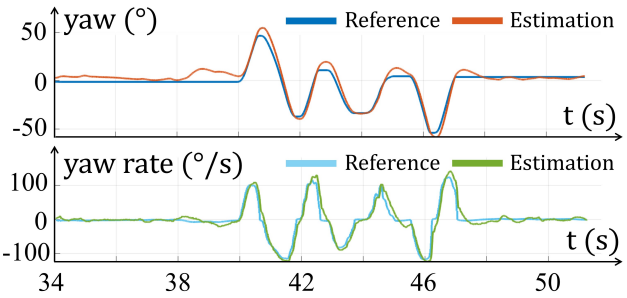

Fig. 13: The result of yaw and yaw rate tracking.

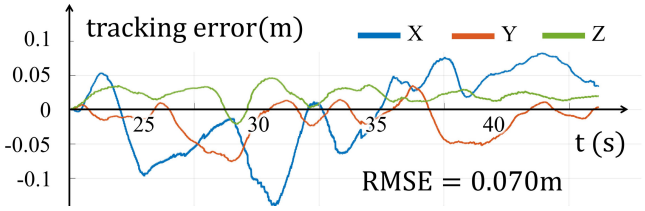

Fig. 14: The tracking error result of autonomous navigation experiment, where the $RMSE$ is $0.070m$.

smartphone. The position setpoint is given by the remote controller. The illustration is shown in Fig. 1(c).

We recommend the readers refer to the attached video for more details of the experiments.

VII. Conclusion

In this work, we first compare the pros and cons among different configurations of rotary-wing aircraft and demonstrate that coaxial helicopters based on control surfaces are the preferred choice for mini UAVs. Afterward, we propose the hardware design of the coaxial helicopter Canfly, with several elaborate mechanisms to minimize its size. Later, we present the dynamic model and control strategy of the proposed system. Finally, abundant experiments are carried out to validate the proposed system's controllability, autonomous ability and traversability, showing its convincing potential to be applied in various fields.

However, there still exist some problems that need further exploration. On the one hand, as the horizontal projection's area decreases, the height of the proposed system increases due to the stacking of the components, which weakens its traversability in the face of horizontal narrow gaps. On the other hand, the arrangement of the mechanism is not optimized, where the air flow inlet of the propeller is partially blocked, resulting in a higher aerodynamic loss. In the future, we aim to optimize the mechanism of Canfly to broaden its application to wider fields.

References

[1] Xin Zhou, Xiangyong Wen, Zhepei Wang, Yuman Gao, Haojia Li, Qianhao Wang, Tiankai Yang, Haojian Lu, Yanjun Cao, Chao Xu, et al. Swarm of micro flying robots in the wild. *Science Robotics*, 7(66):eabm5954, 2022.

[2] Shahin Darvishpoor, Jafar Roshanian, Ali Raissi, and Mostafa Hassanalian. Configurations, flight mechanisms, and applications of unmanned aerial systems: A review. *Progress in Aerospace Sciences*, 121:100694, 2020.

[3] Fei Gao, Luqi Wang, Boyu Zhou, Xin Zhou, Jie Pan, and Shaojie Shen. Teach-repeat-replan: A complete and robust system for aggressive flight in complex environments. *IEEE Transactions on Robotics*, 36(5):1526–1545, 2020.

[4] Wojciech Giernacki, Mateusz Skwierczyński, Wojciech Witwicki, Paweł Wroński, and Piotr Kozierski. Crazyflie 2.0 quadrotor as a platform for research and education in robotics and control engineering. In *2017 22nd International Conference on Methods and Models in Automation and Robotics (MMAR)*, pages 37–42. IEEE, 2017.

[5] Modeling, system identification and robust control of a coaxial micro helicopter. *Control Engineering Practice*, 18(7):700–711, 2010.

[6] Samir Bouabdallah, Roland Siegwart, and Gilles Caprari. Design and control of an indoor coaxial helicopter. In *2006 IEEE/RSJ International Conference on Intelligent Robots and Systems*, pages 2930–2935. IEEE, 2006.

[7] Christian Bermes, Stefan Leutenegger, Samir Bouabdallah, Dario Schafroth, and Roland Siegwart. New design of the steering mechanism for a mini coaxial helicopter. In *2008 IEEE/RSJ International Conference on Intelligent Robots and Systems*, pages 1236–1241. IEEE, 2008.

[8] James Paulos and Mark Yim. Flight performance of a swashplateless micro air vehicle. In *2015 IEEE International Conference on Robotics and Automation (ICRA)*, pages 5284–5289. IEEE, 2015.

[9] James Paulos, Bennet Caraher, and Mark Yim. Emulating a fully actuated aerial vehicle using two actuators. In *2018 IEEE International Conference on Robotics and Automation (ICRA)*, pages 7011–7016. IEEE, 2018.

[10] Zihuan Cheng and Hailong Pei. Flight transition control for ducted fan uav with saturation on control surfaces. In *2021 International Conference on Unmanned Aircraft Systems (ICUAS)*, pages 439–446. IEEE, 2021.

[11] Shuanghou Deng, Siwei Wang, and Zheng Zhang. Aerodynamic performance assessment of a ducted fan uav for vtol applications. *Aerospace Science and Technology*, 103:105895, 2020.

[12] Wayne Johnson. *Helicopter theory*. Courier Corporation, 2012.

[13] Havard Fjaer Grip, Wayne Johnson, Carlos Malpica, Daniel P Scharf, Milan Mandic, Larry Young, Brian Allan, Bérénice Mettler, and Miguel San Martin. Flight dynamics of mars helicopter. 2017.

[14] Larry Lipera, Jason D Colbourne, Mark B Tischler, M Hossein Mansur, Michael C Rotkowitz, and Paul Patangui. The micro craft istar micro air vehicle: Control system design and testing. In *Annual Forum Proceedings-American Helicopter Society*, volume 57, pages 1998–2008. AMERICAN HELICOPTER SOCIETY, INC, 2001.

[15] B. Zhou, F. Gao, L. Wang, C. Liu, and S. Shen. Robust and efficient quadrotor trajectory generation for fast autonomous flight. *IEEE Robotics and Automation Letters*, 4(4):3529–3536, 2019.

[16] Xin Zhou, Zhepei Wang, Hongkai Ye, Chao Xu, and Fei Gao. Ego-planner: An esdf-free gradient-based local planner for quadrotors. *IEEE Robotics and Automation Letters*, 6(2):478–485, 2021.

[17] Gordon J Leishman. *Principles of helicopter aerodynamics with CD extra*. Cambridge university press, 2006.

[18] Youming Qin, Wei Xu, Adrian Lee, and Fu Zhang. Gemini: A compact yet efficient bi-copter uav for indoor applications. *IEEE Robotics and Automation Letters*, 5(2):3213–3220, 2020.

[19] Vinod K Lakshminarayan and James D Baeder. Computational investigation of microscale coaxial-rotor aerodynamics in hover. *Journal of aircraft*, 47(3):940–955, 2010.

[20] Ali Akturk and Cengiz Camci. Tip clearance investigation of a ducted fan used in vtol uavs: Part 1—baseline experiments and computational validation. In *Turbo Expo: Power for Land, Sea, and Air*, volume 54679, pages 331–344, 2011.

[21] Randal W Beard and Timothy W McLain. *Small unmanned aircraft: Theory and practice*. Princeton university press, 2012.

[22] Dario Brescianini, Markus Hehn, and Raffaello D'Andrea. Nonlinear quadrocopter attitude control: Technical report. Technical report, ETH Zurich, 2013.

[23] Daniel Mellinger and Vijay Kumar. Minimum snap trajectory generation and control for quadrotors. In *2011 IEEE International Conference on Robotics and Automation(ICRA)*, pages 2520–2525. IEEE, 2011.

[24] Tong Qin, Peiliang Li, and Shaojie Shen. Vins-mono: A robust and versatile monocular visual-inertial state estimator. *IEEE Transactions on Robotics*, 34(4):1004–1020, 2018.